X-FEM assisted simulation of ductile damage induced 2D crack propagation

Jean-Philippe Crété, Patrice Longère, Jean-Marc Cadou

X-FEM assisted simulation of ductile damage induced 2D crack propagation

Conference Paper · September 2012

CITATIONS
0

READS
12

3 authors:

Jean-Philippe Crété
Supméca - Institut supérieur de mécanique de Paris
15 PUBLICATIONS **19** CITATIONS
SEE PROFILE

Patrice Longère
Clément Ader Institute, Toulouse, France
71 PUBLICATIONS **292** CITATIONS
SEE PROFILE

J.M. Cadou
Université de Bretagne Sud
85 PUBLICATIONS **625** CITATIONS
SEE PROFILE

European Congress on Computational Methods
in Applied Sciences and Engineering (ECCOMAS 2012)
J. Eberhardsteiner et.al. (eds.)
Vienna, Austria, September 10-14, 2012

X-FEM ASSISTED SIMULATION OF DUCTILE DAMAGE INDUCED 2D CRACK PROPAGATION

J.P. Créte[1] [2], P. Longère[1], and J.M. Cadou[2]

[1]Université de Toulouse ISAE/ICA (EA 814)
10 avenue Edouard Belin BP54032 31055 Toulouse cedex 4 France
e-mail: {jean-philippe.crete,patrice.longere}@isae.fr

[2] Université Européenne de Bretagne UBS/LIMATB (EA 4250)
Rue de Saint-Maud´ BP92116 56321 Lorient cedex France
e-mail: jean-marc.cadou@univ-ubs.fr

Keywords: X-FEM, viscoplasticity, damage, computational mechanics

Abstract. *The present work is devoted to the numerical simulation of crack propagation in engineering materials whose failure results from void initiation, growth and coalescence. The behavior of the plate material is described via a Gurson type model accounting for the combined effects of strain hardening, thermal softening, viscoplasticity and void growth induced damage. The eXtended Finite Element Method has been retained to describe the kinematic consequences of the crack propagation across the mesh. The crack is assumed to propagate as soon as the stored energy around the crack tip reaches a critical value. The related crack length is estimated from the crack velocity considering the current time increment. The constitutive model and the extended finite elements were both implemented in the engineering FE computation code Abaqus as user subroutines. The numerical simulation of a notched plate under tension loading has been conducted. While making some simplifications, the present work reproduces numerically the 2D propagation of a crack resulting from void growth induced damage.*

1 INTRODUCTION

The present work is devoted to the numerical simulation of crack propagation in engineering materials whose failure results from ductile damage The fracture of ductile materials is known to result from void initiation, growth and coalescence. During the process of void growth induced damage, the bulk material is subject to a progressive loss of its overall properties and to the appearance, in addition to the isochoric plastic deformation due to dislocation glide in the matrix material, of an inelastic dilatancy due to void growth. In order to describe these effects, the behavior of the material at stake is described via a modified version of the micromechanics based Gurson model, see Gurson ([4]), Tvergaard and Needleman ([5]) and Longère et al ([6]), accounting for the combined effects of strain hardening, thermal softening, viscoplasticity and void growth induced damage.
The numerical treatment of crack propagation in structures is not trivial. The first attempts to achieve it mainly consisted in meshing very finely the crack front to reproduce as accurately as possible the stress-displacement fields at the crack tip. This method implies a very large number of meshes and may be prohibitive when applied to engineering complex structures. Very recently, methods consisting in enriching the finite element kinematics to account for the aforementioned singular fields at the crack tip have emerged. One of these methods, namely the eXtended Finite Element method (X-FEM) [3], has been here retained to describe the kinematic consequences of the crack propagation across the mesh. In the present work, the crack is assumed to propagate as soon as the stored energy around the crack tip reaches a critical value. The related crack length is estimated from the crack velocity considering the current time increment. To estimate the ability of the adopted approach, the numerical simulation of a notched plate under tension loading has been conducted employing the engineering FE computation code Abaqus [13]. While making some simplifications, the present work reproduces numerically the 2D propagation of a crack resulting from void growth induced damage. The constitutive model and the extended finite elements were both implemented in the computation code Abaqus as user subroutines.
The constitutive model of the material considered in the present study is outlined in Sect.2. The finite element enrichment technique adopted in the present work is described in Sect.3. The combination of the constitutive model with the finite enrichment method is detailed in Sect.4. The application of the approach to the numerical simulation of the tension loading of a notched plate is shown and commented in Sect.5.

2 MATERIAL CONSTITUTIVE MODELLING

2.1 Constitutive equations

The failure of the material considered in the present work is supposed to result from void initiation, growth and coalescence. To reproduce the process of ductile damage at stake, the material behavior is described via a Gurson type model, extended by Tvergaard and Needleman. The GTN damage-plastic potential may be written as :

$$\Phi_{GTN} = (\frac{\sigma_{eq}}{\overline{\sigma_y}})^2 + 2q_1 f \cosh(-\frac{3}{2}q_2\frac{p_m}{\overline{\sigma_y}}) - (1 + q_3 f^2) = 0 \tag{1}$$

where σ_{eq} represents the equivalent stress, p_m the pressure, $\overline{\sigma_y}$ the rate dependent yield stress, f the volume fraction of voids, and where (q_1, q_2, q_3) are material constants. Motivated by physical considerations, Longère et al [6] recently introduced in GTN model a mean stress provoking

a shift of the yield locus towards negative stress triaxialities allowing to describe damage growth under shear dominated loading. The modified damage-plastic potential is accordingly proposed in the form :

$$\Phi_{GTN} = (\frac{\sigma_{eq}}{\overline{\sigma_y}})^2 + 2q_1 f \cosh(-\frac{3}{2}q_2\frac{p_m + p_r}{\overline{\sigma_y}}) - (1 + q_3 f^2) = 0 \tag{2}$$

$$p_r = b\ln(q_1 f) \tag{3}$$

with b a positive constant value. The yield stress $\overline{\sigma_y}$ accounts for the combined effects of strain hardening, thermal softening and viscoplasticity :

$$\overline{\sigma_y}(\kappa, \dot{\kappa}, T, ...) = \sigma_y(\kappa, T) + \sigma_{vp}(\dot{\kappa}, T, ...) \tag{4}$$

where κ represent the matrix plastic strain, $\dot{\kappa}$ the matrix plastic strain rate and T absolute temperature. In the rate independent yield stress $\sigma_y(\kappa, T)$, the isotropic strain hardening is described via a Voce type law and the thermal softening via a power law :

$$\sigma_y = (R_0 + R_\infty[1 - \exp(-k\kappa)]^\beta)\left(1 - \left(\frac{T}{T_{ref}}\right)^m\right) \tag{5}$$

where (R_0, R_∞, k, β) are isotropic hardening related constants and (T_{ref}, m) thermal softening related constants. The strain rate induced overstress reproduces the potential tension/compression asymmetry ([7]) :

$$\sigma_{vp} = Y[\dot{\kappa}\exp(\frac{V_a p_m}{k_b T})]^{\frac{1}{n}} \tag{6}$$

where (Y,n) are viscosity related constants and (V_a,k_B) behaviour asymmetry related constants, with $V_a = V_h\beta^3$ where V_h is a constant and β Burgers vector magnitude (β=2.5Å), and with k_B Boltzmann constant (k_B=1.3804.10$^-$23J/K). Assuming the normality rule, the evolution laws are expressed as:

$$\underset{\sim}{d}^p = \Lambda\frac{\partial\Phi_{GTN}}{\partial\underset{\sim}{\sigma}} = \Lambda(\frac{\partial\Phi_{GTN}}{\partial\sigma_{eq}}\underset{\sim}{n} - \frac{1}{3}\frac{\partial\Phi_{GTN}}{\partial p_m}\underset{\sim}{\delta}) = \dot{\epsilon}^{pD}\underset{\sim}{n} + \frac{1}{3}\dot{\epsilon}^{pM}\underset{\sim}{\delta} \tag{7}$$

$$\underset{\sim}{n} = \frac{3}{2}\frac{\underset{\sim}{s}}{\sigma_{eq}} \tag{8}$$

where the distortional and dilatational parts, namely $\dot{\epsilon}^{pD}$ and $\dot{\epsilon}^{pM}$, respectively, of the inelastic strain rate $\underset{\sim}{d}^p$ are given by

$$\dot{\epsilon}^{pD} = \Lambda\frac{\partial\Phi_{GTN}}{\partial\sigma_{eq}} = 2\Lambda\frac{\tilde{\sigma}_{eq}}{\overline{\sigma_y}} \tag{9}$$

$$\dot{\epsilon}^{pM} = -\Lambda \frac{\partial \Phi_{GTN}}{\partial p_m} = 3q_1 q_2 f \Lambda \frac{\sinh[-\frac{3}{2} q_2 (\tilde{p}_m + \tilde{p}_r)]}{\overline{\sigma_y}} \tag{10}$$

with $\tilde{\sigma}_{eq} = \frac{\sigma_{eq}}{\overline{\sigma_y}}$, $\tilde{p}_m = \frac{p_m}{\overline{\sigma_y}}$ and $\tilde{p}_r = \frac{p_r}{\overline{\sigma_y}}$. The evolution law of the isotropic hardening variable κ is deduced from the equality of the macroscopic plastic work rate with the microscopic one, see Gurson ([4]) :

$$\dot{\kappa} = \frac{\sigma_{eq} \dot{\epsilon}^{pD} - p_m \dot{\epsilon}^{pM}}{(1-f)\overline{\sigma_y}} \tag{11}$$

According to the aforementioned considerations, adiabatic heating under dynamic evolution is evaluated from

$$\rho C \dot{T} = \sigma_{eq} \dot{\epsilon}^{pD} - p_m \dot{\epsilon}^{pM} - r\dot{\kappa} \tag{12}$$

The porosity rate $\dot{f}$ is decomposed into a contribution due to growth of existing defects, namely $\dot{f}_g$, and a contribution due to the formation of new defects, namely $\dot{f}_n$:

$$\dot{f} = \dot{f}_g + \dot{f}_n \tag{13}$$

$$\begin{aligned} \dot{f}_g &= (1-f)\mathrm{Tr}\underset{\sim}{d}^p = (1-f)\dot{\epsilon}^{pM} \\ \dot{f}_g(0) &= f_0 \end{aligned} \tag{14}$$

$$\begin{aligned} \dot{f}_n &= B\dot{\sigma_y} \\ \dot{f}_n(0) &= 0 \end{aligned} \tag{15}$$

$$B = f_{sup} \frac{p}{\sigma_c} \Phi_{Io}^{p-1} \exp(-\Phi_{Io}^p) \tag{16}$$

where p is a constant (p=2) and where f_{sup} represents the upper bound of the nucleated secondary void volume fraction. Φ_{Io} is the hole nucleation criterion, see Longère & al. ([6]).

2.2 Numerical procedure

The material behavior outlined in the previous subsection is implemented as user material (UMAT) in the engineering finite element computation code Abaqus. The numerical integration is achieved using the classical return mapping procedure combined with the Newton-Raphson solving algorithm, see Aravas ([10]) for further details. Time increments are small and the tangent operator is elastic. Dividing Eq.(9) by Eq.(10), or inversely, allows for eliminating the viscoplastic multiplier and defining from the incremental viewpoint :

$$\Xi_\Delta = \Delta\epsilon^{pD} \frac{\partial \Phi_{GTN}}{\partial p_m} + \Delta\epsilon^{pM} \frac{\partial \Phi_{GTN}}{\partial \sigma_{eq}} = 0 \tag{17}$$

The numerical integration consists thus in solving the following system of equations

$$\Phi_{GTN}(\sigma_{eq}, p_m; H^\alpha) = 0 \tag{18}$$

$$\Xi_\Delta = 0 \tag{19}$$

$$p_m = p_m^e + K\Delta\epsilon^{pM} \tag{20}$$

$$\sigma_{eq} = \sigma_{eq}^e - 3\mu\Delta\epsilon^{pD} \tag{21}$$

$$\Delta H = h(\Delta\epsilon^{pD}, \Delta\epsilon^{pM}, \sigma_{eq}, p_m, H) \tag{22}$$

where σ_{eq}^e and p_m^e represent the trial, equivalent stress and pressure respectively, and ΔH the system of complementary laws Eqs.(9)-(10) and Eqs.(35)-(16) written in the incremental form. The constants K and μ represent the bulk and shear moduli respectively. Adiabatic conditions are assumed for strain rates greater than $1s^{-1}$.

3 FE ENRICHMENT

3.1 Principle

The extended finite element method (X-FEM) [3] consists in embedding strong discontinuities, induced by e.g. cracks, inside finite elements while enriching the regular displacement of the affected finite elements with singular functions attempting to reproduce the kinematic consequences of the discontinuities at stake. The current displacement field $u(x,t)$ is generally expressed as :

$$u(x,t) = \sum_{i\in I} u_i(t)N_i(x) + \sum_{j\in J} b_j(t)N_j(x)H(x) + \sum_{k\in K} N_k(x)\left(\sum_{l=1}^{4} c_k^l(t)F_l(x)\right) \tag{23}$$

where $u_i(t)$ represents the regular nodal displacement of node i, $b_j(t)$ the discontinuous nodal displacement magnitude of node j belonging to a crack-crossed finite element, and $c_k^l(t)$ the singular nodal displacement magnitude of node k belonging to a crack tip-containing finite element. $N_i(x)$ represent the shape functions, $F_l(x)$ the four singular functions at the crack tip, and $H(x)$ the generalized Heaviside funtion with $H(x) = sign(d_\Gamma(x))$ where $d_\Gamma(x)$ denotes a signed distance function from the crack ($H(x)$ takes the value +1 for the nodes located above the crack and -1 for the nodes located below the crack). The total set of nodes is denoted as I, the set of nodes belonging to crack-crossed finite elements as J, and the set of nodes belonging to crack tip-containing finite elements as K, see 1. In the case of a two-dimensional (2D) elastic problem, the singular functions $F_l(x)$ are expressed in a cylindrical frame (r,θ) as:

$$F_{l=1,2,3,4}(r,\theta) = [\sqrt{r}sin\frac{\theta}{2}, \sqrt{r}cos\frac{\theta}{2}, \sqrt{r}sin\theta sin\frac{\theta}{2}, \sqrt{r}sin\theta cos\frac{\theta}{2}] \tag{24}$$

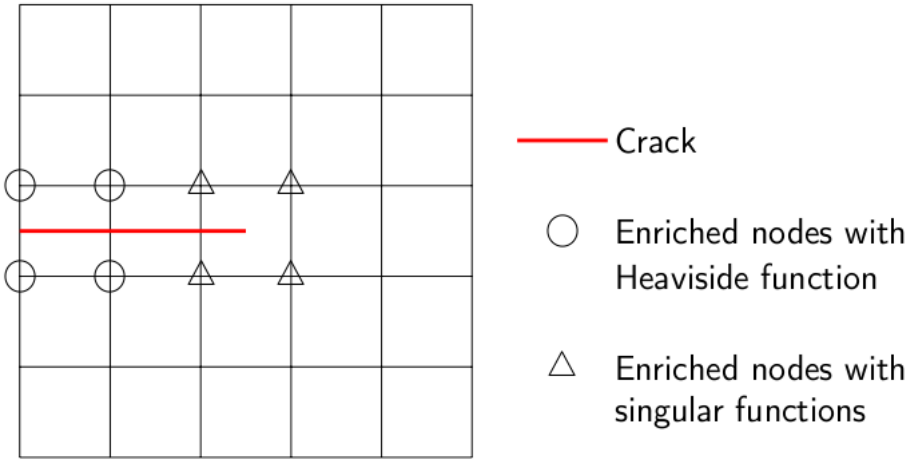

Figure 1: Principle of designation of enriched nodes

3.2 Adopted approach

Regarding the singular displacement field at the crack tip

The X-FE method is particularly efficient when applied to 2D problems involving elastic-brittle materials for which the singular functions $F_l(x)$ can be determined analytically, see Eq.(24). Dealing with elastic-(visco)plastic materials makes the resolution much more difficult because the aforementioned singular functions are generally not a priori known. In certain cases, the functions may be approximated by analytical studies considering simplified material behaviors or by numerical simulations. The fact that the material of the present study is subject to strain hardening, thermal softening, viscoplasticity and ductile damage, see Sect.2, increases significantly the complexity of the singular functions in question. An alternative way consists in using the singular functions defined in the elastic context so as to represent the presence of crack in the element containing the crack tip. Using only the Heaviside function without other enrichment functions, the crack grows element by element, i.e. the crack tip is always located on an edge of an element, so the position of the crack tip is approximate and the field the near crack tip can be perturbed. Fig.2 represents the evolution of the equivalent stress which is averaged over a patch near the crack tip, see [8], for an elastic-plastic notched plate under tensile loading. According to Fig.2, using the sole Heaviside function allows to describe the field near the crack tip with lightly finest mesh compared with X-FEM using singular functions. Moreover neglecting the singular functions allows to reduce drastically the required number of degrees of freedom (dof), 48 dof with the singular functions vs. 8 dof with the sole Heaviside function.

In absence of knowledge of the singular functions for the complex material behavior considered in the present work, and according to the aforementioned remarks, we are here using the reduced current displacement field

$$u(x,t) = \sum_{i \in I} u_i(t) N_i(x) + \sum_{j \in J} b_j(t) N_j(x) H(x) \tag{25}$$

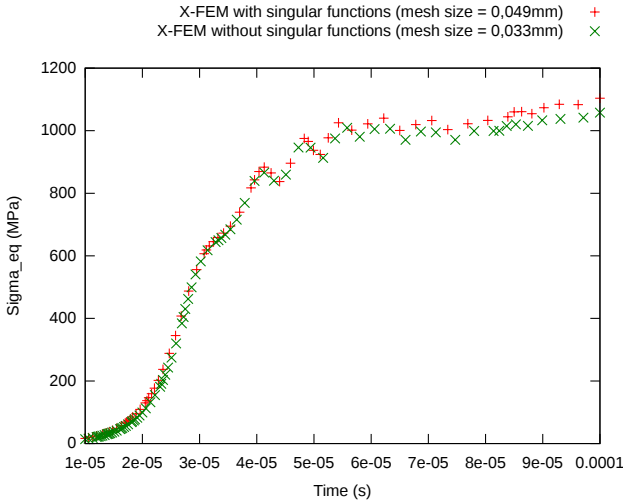

Figure 2: History of the average equivalent stress with and without singular functions. Case of a notched plate submitted to Mode I loading

Regarding the numerical integration

There exist several techniques devoted to capture the crack propagation. The original method consists in subdividing the finite element in which the crack is currently propagating into adaptive sub-triangles, see Fig.3. This however implies re-projecting the state variables values defined at the integration points of the original finite element onto the integration points of the sub-finite elements. The procedure which is easy when dealing with linear evolutions (as it is the case for elastic behavior) is far from being trivial when dealing with non-linear evolutions (it is the case for the present damage-plastic behavior). For this reason, the technique consisting in increasing significantly the number of integration points [1] of the original finite element has been preferred in the present case. We are here using 64 integration points.

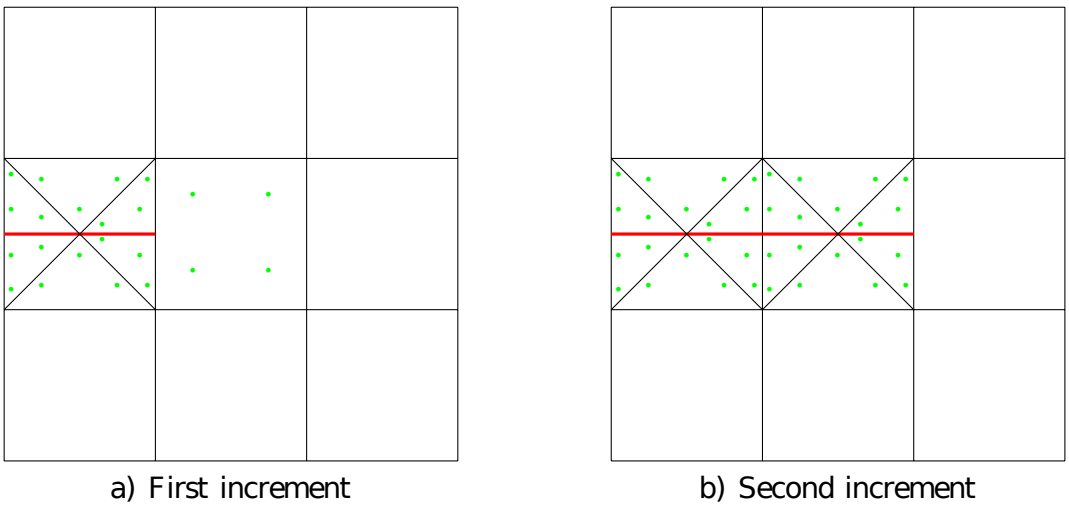

Figure 3: Gauss Points evolution in finite elements during a crack growth

Concerning the nodes belonging to cut and uncut finite elements

To ensure that the enrichment vanishes in all elements not cut by the crack, see [2], the current displacement field $u(x,t)$ takes thus the form

$$u(x,t) = \sum_{i \in I} u_i(t) N_i(x) + \sum_{j \in J} b_j(t) N_j(x)(H(x) - H(j)) \tag{26}$$

where $H(j)$ corresponds to the global discontinuous step function at node j.

4 Coupling X-FEM and ductile damage

The physical process of crack formation being very complex, in particular the transition between the stages of void coalescence and crack germination, we are here tentatively assuming that the transition in question is instantaneous. To avoid too strong mesh size dependence, we are adopting a damage-crack transition criterion based on the stored energy, averaging over a patch at the crack tip. The patch method has notably been used by Haboussa & al.([8]) involving a mean stress based criterion.

4.1 Crack propagation criterion

The instantaneous material state is supposed to be well described via the Helmholtz free energy $\omega(\underset{\sim}{\epsilon}^e, \kappa, T)$ where $\underset{\sim}{\epsilon}^e$ represents the elastic strain tensor. The Helmholtz free energy is decomposed into a reversible and a stored part, namely $\omega_r(\underset{\sim}{\epsilon}^e)$ and $\omega_s(\kappa, T)$ respectively:

$$\omega(\underset{\sim}{\epsilon}^e, \kappa, T) = \omega_r(\underset{\sim}{\epsilon}^e) + \omega_s(\kappa, T) \tag{27}$$

According to the constitutive model outlined in Sect.2, the two contributions to the Helmholtz free energy are expressed as

$$\begin{aligned} \omega_r(\underset{\sim}{\epsilon}^e) &= \frac{1}{2}\underset{\sim}{\epsilon}^e : \underset{\approx}{C} : \underset{\sim}{\epsilon}^e \\ \omega_s(\kappa, T) &= h(\kappa) g(T) \end{aligned} \tag{28}$$

where $h(\kappa)$ represents the stored energy of cold work and $g(T)$ the thermal softening function. The thermodynamic forces are written as

$$\begin{aligned} \underset{\sim}{\sigma} &= \frac{\partial \omega}{\partial \underset{\sim}{\epsilon}^e} = \frac{\mathrm{d}\omega_r}{\mathrm{d}\underset{\sim}{\epsilon}^e} = \underset{\approx}{C} : \underset{\sim}{\epsilon}^e \\ r &= \frac{\partial \omega}{\partial \kappa} = \frac{\partial \omega_s}{\partial \kappa} = h'(\kappa) g(T) \end{aligned} \tag{29}$$

where r represents the matrix isotropic hardening force. According to Eq.(5), the expressions of the strain hardening and thermal softening functions are given by

$$\sigma_y = R_0 g(T) + r(\kappa, T) \tag{30}$$

$$h'(\kappa) = R_\infty [1 - \exp(-k\kappa)]^\beta \tag{31}$$

$$g(T) = 1 - \left(\frac{T}{T_{ref}}\right)^m \tag{32}$$

From the incremental viewpoint, the value of the stored energy at current step (n+1) is deduced from its value at previous step (n) via

$$\begin{aligned} \omega_s^{n+1} &= \omega_s^n + \Delta\omega_s \\ \Delta\omega_s &= \frac{\partial\omega_s}{\partial\kappa}\Delta\kappa + \frac{\partial\omega_s}{\partial T}\Delta T = h'(\kappa)g(T)\Delta\kappa + h(\kappa)g'(T)\Delta T \end{aligned} \tag{33}$$

This quantity is then averaged over a patch containing a finite number of elements namely, p (according to Eq.(35)), located at the crack tip and in the crack growth direction according to

$$\begin{aligned} W_{patch} &= \frac{1}{A}\sum_{i=1}^{p}\omega_s^i A^i \\ A &= \sum_{i=1}^{p} A^i \end{aligned} \tag{34}$$

where A represents the patch area. Keeping constant the total patch area for configurations involving different mesh sizes allows for reducing the mesh size dependence of the numerical results. The principle is illustrated in Fig.4. The crack propagates if

$$F(W_{patch}) = 1 - \frac{W_c}{W_{patch}} > 0 \tag{35}$$

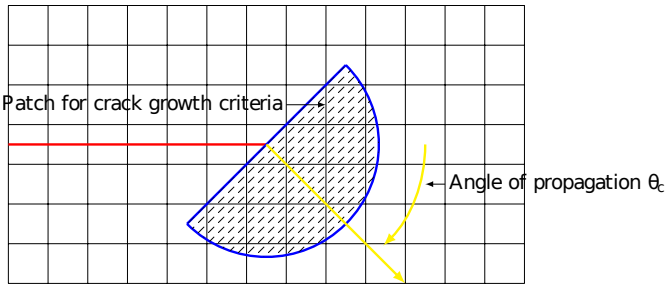

Figure 4: Shape of the patch use for evaluation of the crack growth criteria

4.2 Crack propagation speed

The crack growth rate is estimated using the expression developed by [9] and adapted to the present approach :

$$\dot{a} = C_r F(W_{patch}) = C_r(1 - \frac{W_c}{W_{patch}}) \tag{36}$$

where $\dot{a}$ represents the crack growth rate and C_r the Rayleigh wave celerity in the material. The value of the critical value W_c depends on the material and on the patch radius. From the numerical viewpoint, the crack advance increment is deduced from

$$\Delta a = C_r(1 - \frac{W_c}{W_{patch}})\Delta t \tag{37}$$

4.3 Crack propagation orientation

Identifying the crack propagation orientation constitutes another challenge in the numerical treatment of crack propagation, in particular when dealing with elastic-(visco)plastic materials. Fracture mechanics based criteria, see e.g. Haboussa et al.([8]), as well as bifurcation analyses, see e.g. Hill [11] or Rice [12], are used depending on the application. In a first approach, we used the former works with some modifications. The presence of damage near the crack tip involves a stress drop making the use of the stress field unsuitable from the physics point of view. Therefore an approach based on plastic strain field near the crack tip seems to be more efficient. In a first step, we define a local plastic strain tensor averaged in a patch which is perpendicular to the crack. The crack propagation direction is tentatively deduced from

$$\theta_c = 2\text{arctan}(\frac{1}{4}[\frac{\epsilon^p_{22}}{\epsilon^p_{12}} - sign(\epsilon^p_{12})\sqrt{8 + \frac{\epsilon^p_{22}{}^2}{\epsilon^p_{12}}}) \tag{38}$$

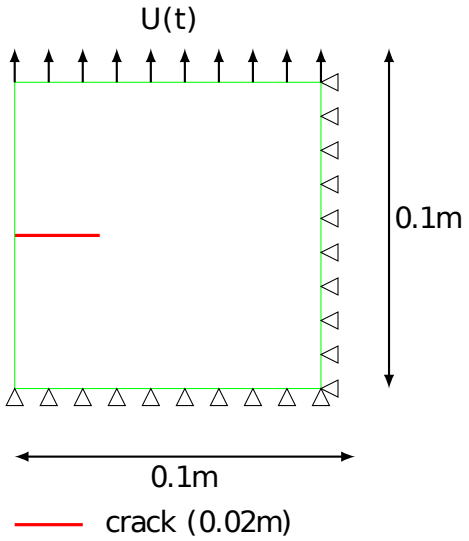

Figure 5: Numerical test of a notched plate under tension loading

5 APPLICATION TO MODE I CRACK PROPAGATION IN A NOTCHED PLATE MADE OF A DUCTILE MATERIAL

To evaluate the prediction ability of our approach, we are considering the crack propagation in a 2D (plane strain) notched plate made of a ductile material, namely the mild steel in Longère et al [6] study, submitted to Mode I loading, see Fig.5. Finite elements are 4 node-quadrilateral with 64 integration points, enriched according to the formulation outlined in Sect.3. The material behavior is described via a user material subroutine integrating the rate equations given in Sect.2. For reason of confidentiality, some constant values are not given. The nodes of the plate upper side are submitted to a constant velocity (1m/s) whereas those of the lower side are constrained.

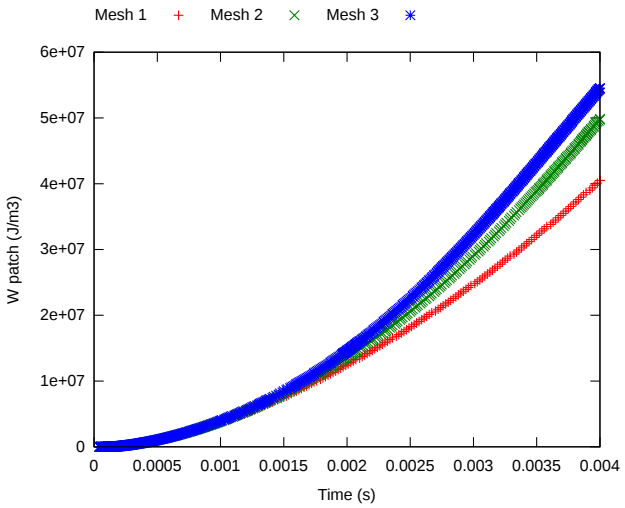

Figure 6: Comparison of the evolution of Wpatch during the test for an angle of 0° for a patch with a radius of 6.25mm

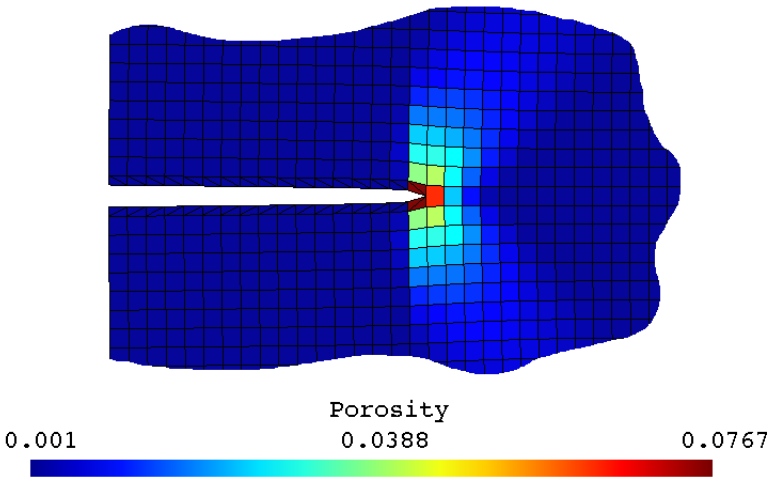

Figure 7: Porosity field for the mesh 1 at 0.001s

5.1 Tension without crack propagation

In a first step, we study the notched plate without crack propagation. The evolution of the energy W_{patch} storaged in a patch (see Eq.35) with a radius of 6.25mm and a angle of 0° for three different mesh size (the mesh 3 is the smallest mesh size and the mesh 1 the most coarse) is drawn in Fig.6. According to Fig.6 one can observe a convergence of the curves which denotes a weak influence of the mesh size on the crack propagation criterion proposed in Sect.4. In Fig.7, the porosity map arround the crack tip at 0.001s is presented. According to Fig.7, the porosity is concentrated near the crack tip, provoking the large mesh dependency observed when a failure porosity is used to represent the crack propagation [14].

The method presented in Sect.4 which allows to propagate a crack, needs two parameters (W_c the crack growth criterion and the radius of the patch). They have to be defined from experimental data. In a first approach, to evaluate the efficiency of the model we use arbitrary values. The crack growth quantity W_c is chosen to be equal to 4.10^6 J.m^{-3} and the radius value of the patch used to definine the crack propagation direction is 6.25mm.

5.2 Tension with crack propagation

The history of the upper side reaction force for configurations with and without crack propagation are drawn in Fig.8. According to Fig.8, one can clearly observe that the crack propagation provokes a drop in the plate response, as expected.

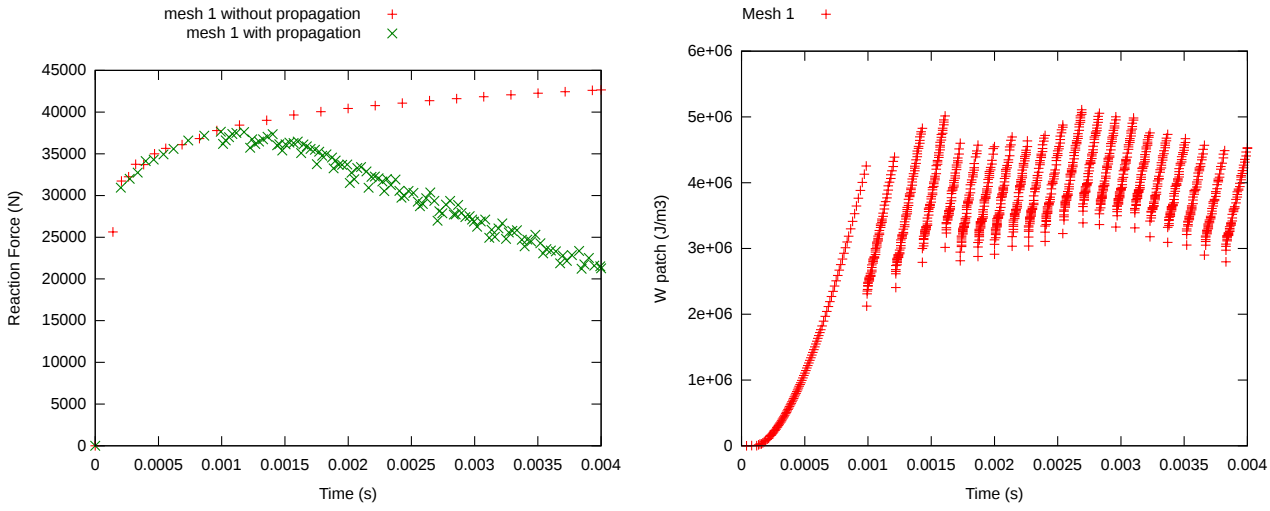

(a) (b)

Figure 8: a) Evolution of reaction force with and without propagation and b) Evolution of Wpatch during crack growth

The evolution of the averaged stored energy W_{patch} is presented in Fig.8. According to Fig.8, Wpatch increases with the increasing displacement (or time), reaches W_c, rises above W_c, then drops suddenly to a value below W_c, then increases, reaches W_c and repeats the aforementionned scenario. The sequential evolution of Wpatch may be explained by the need for the crack to cut completely the element. Refining the mesh size would reduce the magnitude of the fluctuations of Wpatch around Wc and smooth the evolution.

The map porosity in the plate at 4ms is drawn in Fig.9. According to Fig.9, the porosity is concentrated along the crack and as expected the crack growth follows an angle of 0 approxi-

mately. One can observe numerical artefacts consisting in a concentration of porosity in the two corners of the plate which are due to boundary conditions.

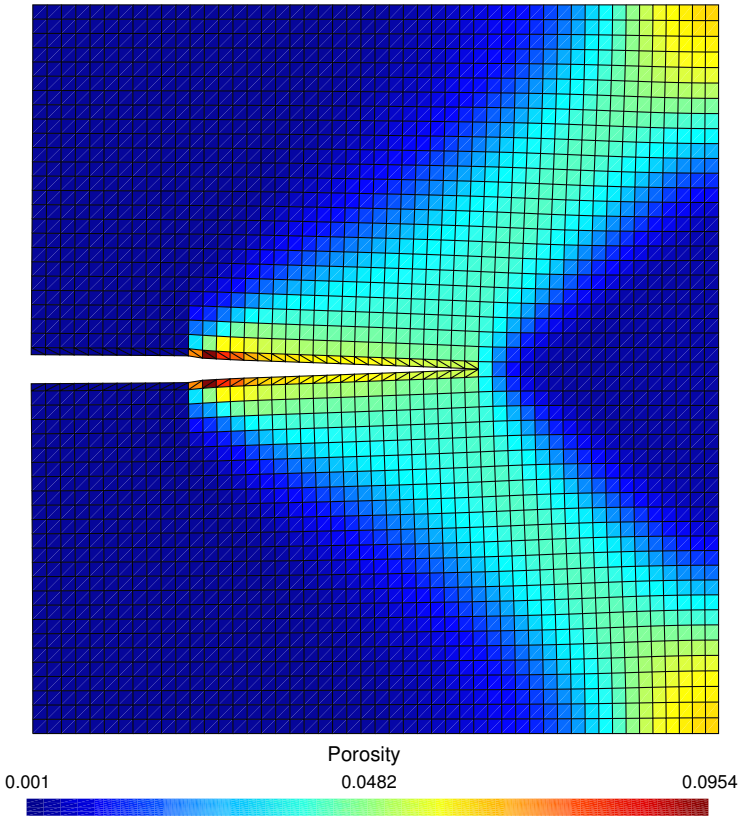

Figure 9: Porosity field at time 0.004s

6 CONCLUDING REMARKS

- This work is devoted to the numerical simulation of crack propagation in engineering materials whose failure results from void initiation, growth and coalescence.
- Our numerical approach coupled a Gurson material ([4], [5]) behavior type with extended finite element method ([3]) to reproduce the crack propagation in a 2D notched structure submitted to Mode I loading.
- The crack growth criterion is based on the energy stored in a patch located near the crack tip. This criterion based on a patch allows to attenuate the mesh size dependence observed when dealing with softening materials. In a first approach the crack propagation direction is deduced from the plastic strain field near the crack tip. The crack length is defined using the definition introduced in reference ([9]) in adequation with our approach.
- Experimental tests in modes I and II would be very useful to define more accurately the quantities used in our approach.

[1–3]
The Authors would like to aknowledge the financial support of DGA (French Ministry of

Defence) as well as the fruitful discussions with Prof. M. Salaun from Toulouse University, ISAE/ICA, France.

REFERENCES

[1] T. Elguedj, A. Gravouil, A. Combescure: Appropriate extended functions for X-FEM simulation of plastic fracture mechanics. *Computer Methods in Applied Mechanics and Engineering*, 195 (2006), 501–515.

[2] G. Zi, T. Belytschko: New crack-tip elements for XFEM and applications to cohesive cracks. *International Journal for Numerical Methods in Engineering*, 57 (2003), 2221–2240.

[3] N. Moes, J. Dolbow, T. Belytschko: A finite element method for crack growth without remeshing. *International Journal for Numerical Methods in Engineering*, 46 (1999), 131–150.

[4] A.L. Gurson: Continuum theory of ductile rupture by void nucleation and growth: Part I Yield criteria and flow rules for porous ductile media. *Journal of Engineering Materials and Technology*, 99 (1977), 2–15.

[5] V. Tvergaard, A. Needleman: Analysis of the cup-cone fracture in a round tensile bar. *Acta Metallurgica*, 32 (1984), 157–169.

[6] P. Longère, A.G. Geffroy, B. Leblé, A. Dragon: Modelling the Transition between Dense Metal and Damaged (Micro-Porous) Metal Viscoplasticity. *International Journal of Damage Mechanics*.

[7] S. Graff, S. Forest, S. Strudel, J.L. Prioul, P. Pilvin, J.L. Béchade: Strain localization phenomena associated with static and dynamic strain ageing in notched specimens: experiments and finite element simulations. *Materials Science and Engineering*, (2004), 181–185.

[8] D. Haboussa, D. Grégoire, T. Elguedj, H. Maigre, A. Combescure : X-FEM analysis of the effects of holes or other cracks on dynamic crack propagations. *International Journal for Numerical Methods in Engineering*, 86 (2011), 618–636.

[9] M. Kanninen, C.H. Popelar: Advanced Fracture Mechanics. Oxford University Press, 1985.

[10] N. Aravas : On the numerical integration of a class of pressuredependent plasticity models. *International Journal for Numerical Methods in Engineering*, 24 (1987), 1395–1416.

[11] R. Hill: Acceleration waves in solids. *Journal of the Mechanics and Physics of Solids*, 10 (1962), 1–16.

[12] J.R Rice: The Localization of Plastic Deformation. *Koiter, W. (Ed.). Amsterdam, North-Holland*, (1976), 207–220.

[13] D. Hibbitt, B. Karlsson, P. Sorensen : ABAQUS Users Manual, Version 6.9. Hibbitt, Karlsson & Sorensen Inc., 2009.

[14] R. Hambli : Comparison between Lemaitre and Gurson damage models in crack growth simulation during blanking process. *International Journal of Mechanical Sciences*, 43 (2001), 2769–2790.